Preprint of paper published as

Acta Materialia **56**, 2008, 5123-29;

DOI: 10.1016/j.actamat.2008.06.025

The brittle-ductile transition in single-crystal iron

M. Tanaka*, E. Tarleton, S.G. Roberts

Department of Materials, University of Oxford,
Parks Road, Oxford OX1 3PH, UK
*Present address: Department of Materials Science and Engineering,
Kyushu University, 744 Motooka, Fukuoka, 819-0395 JAPAN

Keywords: brittle-ductile transition; fracture; iron; dislocations, dislocation dynamics, modelling.

Abstract

The fracture behaviour of single crystal pure iron was studied by four-point bending of pre-cracked specimens at temperatures between 77K and 180K and strain rates between 4.46×10^{-5} and 4.46×10^{-3} s^{-1}. Fracture behaviour changes from brittle to ductile with increasing temperature. The brittle-ductile transition temperature increases with increasing strain rate. The relation between brittle-ductile transition temperature and strain rate follows an Arrhenius relation, giving an activation energy for the brittle-ductile transition of 0.33 eV. Dislocation-dynamics simulations of the crack-tip plasticity and resultant shielding of the crack tip were performed using two different variants of the dislocation velocity / stress / temperature relation. The models predict an explicit brittle-ductile transition, and give a good quantitative fit to the experimental transition temperatures.

Introduction

Many materials fail in a brittle manner at low temperatures and deform plastically at high temperatures. The most common type of brittle-ductile transition (BDT) observed in many single crystal metals and intermetallics is a "gradual" transition, where the fracture toughness increases gradually over a range of 100K or more between low test temperatures up to the transition temperature, T_c, above which the material is ductile. This type of BDT is seen in, for example, Ge [1], Mo [2,3], W [4], γ-TiAl [5], NiAl [6] and MgO [7]. The other type of transition is "sharp", where the fracture toughness is constant below T_c, and increases rapidly only within a few degrees of T_c; this has been seen in Si [8,9,10,11], Al_2O_3 [12] and Fe-3%Si [13].

For both types of transition, the relation between the strain rate, $\dot{\varepsilon}$, and the transition temperature, T_c, has been found empirically to be given by:

$$\dot{\varepsilon} = A \cdot \exp\left(-E_a / kT_c\right) \tag{1}$$

where A is a pre-factor, k is Boltzmann's constant and E_a is the activation energy for the BDT. In materials where data exist for comparison, the value of E_a is found to be close to the activation energy for dislocation glide, indicating that the BDT in those materials is controlled by dislocation glide [14]. Hirsch, Roberts and Samuels[15] suggested a dislocation-based model of plastic-zone evolution in which dislocations emitted from the crack tip glide away to form a crack-tip plastic zone. Each emitted dislocation reduces the crack-tip stress intensity via elastic interactions (the "shielding" effect). Models of this type have been successful in modelling the changes in fracture toughness with temperature in the brittle regime in many materials [16,17]; however, to model the brittle-ductile transition itself, additional assumptions are required about the origins and behaviour of the dislocation sources (e.g. in Si [15]). These models have also been adapted to model fatigue crack growth [18] and brittle-particle-initiated fracture in steels [19] .

In the present study, the brittle-ductile transition behaviour of pure single crystal iron was investigated, measuring the fracture toughness over a range of temperatures and strain rates. The activation energy for the BDT was derived from the variation of T_c with strain rate, according to equation (1). Dislocation-dynamics simulations of crack-tip plastic zone development were performed using a dislocation velocity law based on a kink-nucleation mechanism[20] (with no prior assumption that the value of the activation energy for the BDT obtained in this study is that for dislocation glide). Simulations were also performed using an empirical velocity law based on the available (very limited) dislocation velocity data for iron [21], using the experimentally-measured activation energy.

Experimental

Iron single crystal was supplied by Metal Crystal and Oxides, Cambridge, UK. Specimens were crystallographically aligned by Laue X-ray diffraction, cut to size using a diamond-bladed wafering saw, and then polished by a succession of diamond pastes on laps and cloths, finishing with an electropolish in 10% perchloric acid and 90% acetic acid. The specimen geometry used was as shown in Figure 1 (a). A notch and pre-crack with total depth of approximately 80 μm was introduced into one surface of each beam by electro-discharge from a sharp edge at room temperature. Four-point bending tests were performed at outer-fibre strain rates of 4.46×10^{-5}, 4.46×10^{-4} and 4.46×10^{-3} s^{-1}. The test temperature was controlled by using liquid nitrogen at 77K and cold nitrogen gas from 100K to 180K; during each test, temperature was controlled to within ±0.5K. Fracture toughness, K_{Ic}, in four-point bending was calculated using the following equation [22]:

$$K_{Ic} = f(\xi)\sqrt{\pi c}\sigma_{frac}, \quad \xi = c / L$$

$$f(\xi) = 1.112 - 1.40\xi + 7.33\xi^2 - 13.08\xi^3 + 14.0\xi^4 \qquad (2)$$

where σ_{frac} is the fracture stress, c is the crack depth and L is the specimen thickness. The crack depth for each specimen was measured after fracture by scanning electron microscope examination of the fracture surface.

Results

Fracture toughness measurements and the activation energy for the BDT

Figure 2 shows fracture toughness as a function of test temperature at strain rates of 4.46×10^{-3}, 4.46×10^{-4} and 4.46×10^{-5} s^{-1}. Each point corresponds to a single test. Solid diamonds indicate that specimens fractured with no plastic deformation visible via the stress strain-curve or in the final specimen shape, and with a planar fracture surface; these were classified as "brittle". Solid squares indicate that the specimens reached 3.5% strain (the test rig's limit) during the test without fracture; these were classified as "fully ductile". (In these cases, the fracture toughness values shown on the figure were calculated using the stress at 3.5% strain and the mean crack size for the brittle specimens (80 μm), and are thus lower limits.) Finally, an intermediate type was observed, where fracture occurred only after a significant amount of plastic deformation (2% or more) and work-hardening; the corresponding tests are marked as solid triangles; such tests were classified as "high-strain fracture".

The mean fracture toughness value for brittle fracture at 77K over all the strain rates used was 11.7 ±1.3 MPa $m^{1/2}$. The brittle ductile transition temperature T_c, indicated by dashed lines in Figure 2, was taken as the median of the highest temperature for brittle fracture and the lowest temperature for either ductile bending or high-strain fracture. Table 1 shows the measured transition temperatures at the three strain rates used; T_c increases with increasing strain rate. The value of fracture toughness at the BDT was found to be larger than at 77K.

Figure 3 shows an Arrhenius plot of reciprocal transition temperature as a function of ln(strain rate), fitting the experimental data to equation (1). The three points obtained at strain

rates of 4.46×10^{-3}, 4.46×10^{-4} and 4.46×10^{-5} s^{-1} are a good fit to a single line, giving an activation energy for the brittle-ductile transition of 0.33 eV.

Crack-tip dislocation activity

Figure 4(a) shows a side view of a sample loaded at a strain rate of 4.46×10^{-4} s^{-1} at 144K, i.e. slightly above T_c. The crack has extended from the original notch root, though without catastrophic fast fracture. Several slip bands along ⟨110⟩ directions are visible around the crack, indicating that dislocations are on $\{1\bar{1}0\}$ planes. Short wavy lines ahead of the straight slip bands indicate that screw dislocations have cross slipped between various glide planes. Figure 4(b) shows a schematic drawing of likely crack-tip dislocation configurations. Dislocation loops with Burgers vector $a/2\langle 11\bar{1}\rangle$ are generated at sources near the crack tip and expand on a $\{1\bar{1}0\}$ slip plane. When dislocation segments with opposite Burgers vectors meet between sources, the reacting segments mutually annihilate, leaving one larger loop. This process repeats producing long approximately straight edge dislocation segments. The screw segments of the dislocation loops can cross-slip to form the wavy slip lines seen in Figure 4(a).

Dislocation dynamics modelling

The model

The dislocations emitted from the crack tip can modify the stress intensity at the crack tip, an effect known as “shielding” if the crack tip stress intensity is reduced by the dislocations and as “antishielding” if it is increased [23]. Direct TEM observations of dislocations generated at crack tips in MgO and Si have shown that dislocations emitted from the crack tip are of the shielding type [24,25]; this is also the sense of dislocations that will be moved away from crack-tip sources by the crack tip stress field (antishielding dislocations are attracted to, and absorbed by, a loaded crack tip)[26]. The shielding effect of dislocations emitted from the crack tip increases the externally applied stress intensity required for fracture.

A simple two-dimensional discrete dislocation dynamics model of the crack tip plastic zone was originated for silicon by Hirsch, Roberts and Samuels [27] and has since been developed and applied to other materials[1,2,5,28,29,30]. In the model, a semi-infinite crack has a mode I stress applied, linearly increasing with time. The crack tip plastic zone is modelled here as a pair of slip planes inclined at an angle $\pm\theta$ to the crack plane, with a dislocation source close to the crack tip lying on each slip-plane (previous models used only a single slip plane on one side of the crack tip). Dislocations are produced at each source if the total stress there positive, and move away along the slip plane, to form a one-dimensional array on each slip plane. The shear stress, τ_i, on the i^{th} dislocation in such an array of dislocations is given by:

$$\tau_i = \frac{K_{app}}{r_i^{1/2}} f(\theta) + \frac{K_{app}}{c^{1/2}} g(r_i, \theta, c, L) + \frac{\mu}{r_i} h(\theta) + \sum_{i \neq j} m\left(\frac{\mu}{|r_i - r_j|}, \theta\right) \qquad (3),$$

where K_{app} is the applied stress intensity factor, r_i is the distance of the dislocation from the tip of the crack (of length c), θ is the angle between the slip plane and the crack plane (45° for these simulations (see Figure 1 (b)), μ is the material's shear modulus, L is the specimen thickness and f, g, h and m are functions of the variables given. The first term is related to the crack-tip stress field, the second term to the specimen bending stress field, the third term to dislocation – image dislocation interactions (to satisfy the zero-stress boundary conditions on the crack surfaces) and the fourth term to dislocation-dislocation interactions. For edge dislocations near a mode I crack, exact solutions for the first, third and fourth terms are given by Lakshmanan and Li [26]; the second term is simple to calculate for a given specimen geometry.

Given the local shear stress, the velocity of each dislocation may be calculated for the temperature being modelled. Iron is a body-centred cubic metal where screw and mixed-type dislocations move much more slowly at a given stress and temperature than pure edge

dislocations [31]. In these simulations, the complex three-dimensional growth of the crack tip plastic zone is modelled in two dimensions; hence the dislocation velocity law used was that of screw dislocations, as their slower motion controls the rate of emission of dislocation loops from dislocation sources[32,33], and as the velocity of screw and mixed dislocations that form most of the loops (see Figure 4 (b)) will determine the positions of the dislocations close to the crack tip that will be responsible for the majority of the shielding. Two types of velocity law were used.

The first velocity law is based on the mechanics of motion of a screw dislocation by nucleation and expansion of double kinks[20]:

$$v = v_0 \exp\left(\frac{-(E_0 - V_A\tau)}{kT}\right) \tag{4}$$

where v_0 is a constant, E_0 is the activation enthalpy to create a double-kink pair at zero stress, and V_A is the activation volume for double-kink formation, typically $\approx 20b^3$ [34]. Brunner *et al.* [35,36,37] obtained a value of E_0 for pure iron by means of stress-relaxation tests, and found that E_0 depends on the temperature range of the test: 0.93 eV above 250K (regime I), 0.74 eV between 120K and 250K (regime II) and 0.60 eV below 120K (regime III). The BDT temperatures found in this study are in regime II, giving an E_0 value of 0.74 eV.

The second velocity law used was empirical, but one that has been found to be applicable to experimental data for a wide range of materials [38]:

$$v = v'_0 \left(\frac{\tau}{\tau_0}\right)^m \exp\left(\frac{-E_m}{kT}\right), \tag{5}$$

where v'_0, τ_0 and m are constants, and E_m is the activation energy for dislocation glide. Assuming that the activation energy for the BDT is that for dislocation glide [14], $E_m = E_a =$ 0.33 eV. For each velocity law, v_0 or v'_0 was adjusted to give best fit to experimental data at

one strain rate (the lowest); the experiments at the higher strain rates were then modelled by keeping the value of v_0 or v'_0 constant and increasing the simulated strain rate.

Due to dislocation shielding the stress intensity at the crack-tip is

$$K_{tip}(t) = K_{app}(t) - K_{dis}(t) = \dot{K}_{app} t - B\sum_{i=1}^{N(t)} r_i(t)^{-1/2} . \quad (6)$$

Where the applied loading rate $\dot{K}_{app} \propto \dot{\varepsilon}$, and $B \propto |\boldsymbol{b}|$ is a positive constant depending on the material and geometry[26]. The dynamic part of the dislocation shielding term depends only on the distance of each dislocation from the crack tip, *r(t)*, and the number of dislocations *N(t).* The Burgers vector $|\boldsymbol{b}| = 0.248\,\text{nm}$ was taken at an angle of 45˚ to the crack plane.

(Simulations were also performed to explore the possible effects of variants in projecting the 3-dimensional plastic zone onto 2-dimensional model. The actual $\boldsymbol{b} = a/2[111]$ is not in the slip plane of the simulation; simulations were also performed using a Burgers vector length equal that of a/2[111] projected onto the $(0\bar{1}0)$ plane of the simulations. This amounts to setting $\boldsymbol{b}$' = a/2[101] = $(2/3)^{1/2}$ $\boldsymbol{b}$. This gives reduced interaction stresses between the dislocations, resulting in the number of dislocations at a given applied stress intensity increasing by $(3/2)^{1/2}$, so the overall shielding effect and the results of the simulations were unchanged; hence the results of such calculations are not given explicitly in this paper.)

Modelling Results

Figure 5 shows crack-tip stress intensity $K_{tip} = K_{app} - K_{dis}$ (i.e. applied stress intensity minus the effect of dislocation shielding) as a function of applied stress intensity K_{app}, at a strain rate of 4.46×10^{-5} s^{-1}, using the kink-pair velocity law. The crack size in the simulation was 80 μm, and the specimen thickness was 1 mm (the values used in experiments). The crack-tip stress intensity K_{tip} reaches a peak value before decreasing with further applied loading. This is because the applied strain rate and hence applied stress intensity factor application rate,

dK_{app}/dt, is a constant, whereas the dislocation nucleation rate and hence shielding rate dK_{dis}/dt increases with time, eventually exceeding dK_{app}/dt. It is clear from (6) that the peak in $K_{tip}(t)$ occurs when

$$\frac{dK_{dis}}{dt} = \frac{dK_{app}}{dt} \quad \textbf{or} \quad \frac{dK_{dis}}{dK_{app}} = 1 \quad . \tag{7}$$

As the simulated temperature is increased, the dislocation nucleation rate and hence the dislocation shielding at a given K_{app} increases, hence K_{tip} decreases; see Figure 5.

If the loading rate and temperature are such that K_{tip} exceeds the pure-cleavage fracture toughness of the material K_{Ic} before the peak in K_{tip} is reached then the material is assumed to fracture. The value of K_{app} at which this occurs, here termed K_F, will be greater than K_{Ic} because of the effects of dislocation shielding; see eqn. (6). As the simulated temperature is increased, the increasing mobility of the dislocations allows more rapid nucleation from each source, and hence increased shielding which delays fracture, resulting in a larger value of K_F. Above a critical temperature (130 K at a strain rate of 4.46×10^{-5} s^{-1}, the peak in K_{tip} falls below the cleavage fracture toughness of the material K_{Ic}, and fracture cannot occur. Eventually the maximum applied stress on the specimen, $\sigma_{app} = (\pi c)^{-1/2} K_{app}$, exceeds the yield stress, σ_y (see Figure 5) and thus the simulation predicts ductile behaviour. Hence the condition for the brittle-ductile transition is that the peak value of $K_{tip}(t) = K_{Ic}$. To meet this condition as the applied loading rate is increased, the rate of shielding from the emitted dislocations must increase, hence the predicted brittle-ductile transition temperature must also increase (Figure 6).

The value of K_{Ic} was assumed to be the Griffith value, $(2\gamma E)^{1/2}$, with Young modulus E = 211 GPa and a free surface energy value, γ, of 2.2 Jm^{-2} as calculated for Fe using density functional theory by Vitos et al [39], giving K_{Ic} = 1 MPa $m^{1/2}$.

Simulation results

Double-kink based velocity law

The parameters used for the double-kink based velocity law (4) were: E_0 = 0.74 eV, activation volume $V_A = 20\ b^3$, where b is the Burgers vector (248 pm). The constant v_0 was set so that the model gave the same transition temperature as found experimentally at the lowest strain rate used (130 K at $4.46 \times 10^{-5}\ s^{-1}$), giving $v_0 = 8 \times 10^{13}\ ms^{-1}$. The predictions of the model for the higher strain rates, $4.46 \times 10^{-4}\ s^{-1}$ and $4.46 \times 10^{-3}\ s^{-1}$, are shown in Figure 6 and Table 1. The model gives values of transition temperature in good agreement with the experiments. The shape of the $K_F\ (T)$ profile obtained is sharp and this is in good agreement with the experimental observations shown in Figure 2, though the predicted "lower shelf" values of K_F are lower than those found experimentally. The net shear stress on dislocations was found not to vary greatly either with their position in the dislocation array, or with time, and was approximately 140 MPa at all three strain rates. This implies the effective activation energy $E_a = E_0 - V_A \tau \approx 0.48$ eV.

Empirical velocity law

Simulations were also performed using the empirical velocity law given in equation (5) with constant values for τ_0 = 1 MPa, E_a = 0.33 eV and the stress exponent, m = 4 (from the available experimental data [21]). The velocity pre-factor $v_0 = 0.32\ ms^{-1}$ was set by matching the predicted to the experimental brittle-ductile transition temperature at the lowest strain rate (130K at $4.46 \times 10^{-5}\ s^{-1}$). The results of modelling using these parameters are shown in Figure 6. The predicted transition temperatures at the two higher strain rates are in agreement with experimental values (as would be expected since the experimentally-derived activation energy is used), and again the shape of the predicted transition is "sharp" in accord with experiments, though with a lower fracture toughness at low temperatures.

Discussion

The models, using two different dislocation velocity laws, give good agreement with experimental data and with each other. The models use parameters (geometry, strain rate, activation energies, etc.) taken directly from experimental values; the only freely adjustable parameters are the velocity law pre-factors v_0 and v'_0 for the two velocity laws.

In the experimental work, specimens that fractured only after significant amounts of plastic deformation and work-hardening ("high-strain fracture") were classified with the "fully ductile" specimens when determining the brittle-ductile transition temperature, which was set at a temperature between this group of results and those where cleavage fracture occurred. Such work-hardening is not taken account of in the models, where the dislocations move in a "laminar flow" mode on their glide planes, and so this eventual fracture after work-hardening is not predicted.

The empirical velocity law, using an activation energy for dislocation motion equal to that derived from the fracture experiments, exactly predicts the transition temperatures at higher strain rates, demonstrating that this type of model gives a self-consistent picture of the phenomena controlling the brittle-ductile transition. The kink-pair velocity law gives predictions very close to the experimental values. (The transition temperatures predicted using the double-kink law are a good fit, within the (small) experimental errors, to the transition temperatures found experimentally.) The model shows that the dislocations in the crack-tip plastic zones self-organise so that the dislocation arrays have nearly constant internal shear stress, giving an effective activation energy for motion, lower than the zero-stress activation energy for double-kink nucleation, that is close to the activation energy obtained from fracture data experiments.

Summary and Conclusions

The brittle-ductile transition (BDT) behaviour of single crystal iron was investigated using a four-point bending method. The BDT temperature increased with increasing strain rate. An Arrhenius plot between the strain rate and reciprocal transition temperature gives an activation energy for BDT of 0.33eV. The experiments were modelled using two dimensional crack-dislocation dynamics simulation. The models predict an explicit brittle-ductile transition. The transition occurs at the temperature where the shielding effect of dislocations emitted from the crack tip increases sufficiently rapidly to prevent the crack-tip stress intensity reaching the cleavage fracture toughness of the material. The models give a good quantitative description of the brittle-ductile transition temperature and its variation with loading rate.

Acknowledgements

The work reported here was supported financially by the EPSRC under research grant GR/M058811 and by UKAEA Culham Laboratory. We gratefully acknowledge useful discussions with Prof. S.L. Dudarev, Dr. A. Giannattasio and Dr. R. Novokshanov.

Figure Captions

Figure 1: (a) Specimen geometry used in four-point bend fracture tests of single crystal iron. (b) The 2D model consists of a pair of slip planes at an angle $\theta = 45°$ to the crack plane. Dislocations are nucleated at the two sources (dotted) placed 30 b from the crack-tip and move away from the tip allowing two dislocation arrays to form.

Figure 2: Experimental fracture toughness of single crystal iron as a function of test temperature at strain rates of: (a) 4.46×10^{-3} s^{-1}, (b) 4.46×10^{-4} s^{-1}, (c) 4.46×10^{-5} s^{-1}.

Figure 3: Arrhenius plot of reciprocal transition temperature in single crystal iron as a function of ln(strain rate).

Figure 4: (a) Side view of a specimen tested at 144K and 4.46×10^{-4} s^{-1} (slightly above T_c). Two types of slip bands are visible: straight lines aligned along <110> directions and wavy lines indicating cross slip. (b) probable crack-tip dislocation configurations.

Figure 5: Predicted crack tip stress intensity K_{tip} as a function of applied stress intensity K_{app} at different temperatures at a loading rate of 4.46×10^{-5} s^{-1} Above a critical temperature (130 K in the figure), the fracture condition $K_{tip} = K_{Ic}$ is never met and the material is predicted to be ductile. Below this critical temperature, fracture is predicted to occur at an applied stress intensity $K_{app} = K_F$, higher than K_{Ic} due to the effects of dislocation shielding.

Figure 6: Experimental and modelled fracture toughness of single crystal iron as a function of test temperature at strain rates of: (a) 4.46×10^{-3} s^{-1}, (b) 4.46×10^{-4} s^{-1}, (c) 4.46×10^{-5} s^{-1}.

References

1. Serbena FC, Roberts SG. Acta Metall Mater 1994;42:2505
2. Roberts SG, Ellis M, Hirsch PB. Mat Sci and Eng A 1993;164:135
3. Gumbsch P, Riedle J, Hartmaier A, Fischmeister HF. Science 1998;282:1293
4. Giannattasio A, Roberts SG. Phil Mag 2007;87:2589
5. Booth AS, Roberts SG. Acta Mater 1997;45:1045
6. Serbena FC. D.Phil thesis. University of Oxford 1995
7. Roberts SG, Ellis M, Hirsch PB. Mat Sci and Eng A 1993;164:135
8. St. John C. Phil Mag 1975;32:1193
9. Samuels J, Roberts SG. Proc R Soc Lond A 1989;421:1
10. George A, Champier G. Phys Stat Sol A 1979;53:529
11. Brede M, Haasen P. Acta Metall 1988;36:2003
12. Kim HS, Roberts SG. J Am Ceram Soc 1994;77:3099
13. Ha KF, Yang C, Bao JS. Scripta Metall Mat 1994;30:1065
14. Giannattasio A, Tanaka M, Joseph TD, Roberts, SG. Physica Scripta T 2007;128:87.
15. Hirsch PB, Roberts SG, Samuels J. Proc R Soc Lond A 1989;421:25
16. Hirsch PB, Roberts SG. Phil Trans Roy Soc 1997;355:1991
17. Roberts SG. Modelling the brittle to ductile transition in single crystals. In: Kirchner HO, Kubin LP, Pontikis V, editors. Computer Simulation in Materials Science - nano / meso / macroscopic space and time scales, NATO ASI series, series E (applied sciences), vol. 308. Kluwer Academic Publishers, The Netherlands, 1996. p.409.
18. Wilkinson AJ, Roberts SG. Scripta Mat. 1996;35:1365
19. Roberts SG, Noronha SJ, Wilkinson AJ, Hirsch PB. Acta Mater. 2002;50:1229
20. Seeger A. J Physique 1981;42:201
21 Turner APL, Vreeland T. Acta Met 1970;18:1225

22. Brown WF, Srawley JE. ASTM STP 1966;410:1

23. Majumdar BS, Burns SJ, Acta Metall 1981;29:579

24. Higashida K, Narita N, Asano S, Onodera R. Mat Sci & Eng A 2000;285:111

25. Tanaka M, Higashida K. Mat Sci & Eng A 2005;400-401:426

26. Lakshmanan V, Li JCM. Mat Sci & Eng A 1988;104:95

27. Hirsch PB, Roberts SG, Samuels J. Scripta Met 1987;21:1523

28. Hirsch PB, Roberts SG. Phil Mag 1991;64:55

29. Wilkinson AJ, Roberts SG. Scripta Mat. 1996;35:1365

30. Roberts SG. Modelling brittle-ductile transitions. In: Lepinoux J, Maziere D, Pontikis P, editors. Multiscale Phenomena in Plasticity: From Experiments to Phenomenology, Modelling and Materials Engineering, vol 367. Kluwer Academic Publishers, The Netherlands, 2000. p.349.

31 Urabe N, Weertman J. Mat Sci Eng 1975;18:41

32 Jouiad M, Lagow BW, Robertson IM, Lassila DH. In-situ TEM deformation studies of dislocation generation and motion in high-purity Mo single crystals. In: Lassila DH, Robertson IM, Phillips R, Devincre B. Multiscale Phenomena in Materials-Experiments and Modeling, vol 578. MRS Conf series, Material Research Society, 2000. p.113

33 Tang M, Fivel M, Kubin LP. Mat Sci & Eng A 2001;309:256

34 Mordike BL, Hassen P. Phil Mag 1962;7:459

35. Brunner D, Diehl J. Phys Stat Sol (a) 1991;124:155

36. Brunner D, Diehl J. Phys Stat Sol (a) 1991;124:203

37. Brunner D, Diehl J. Phys Stat Sol (a) 1991;124:455

38. Nadgornyi E. Prog Mat Sci 1988;31:1

39. Vitos L, Ruban AV, Skriver HL, Kollar J. Surf Sci 1998;411:186

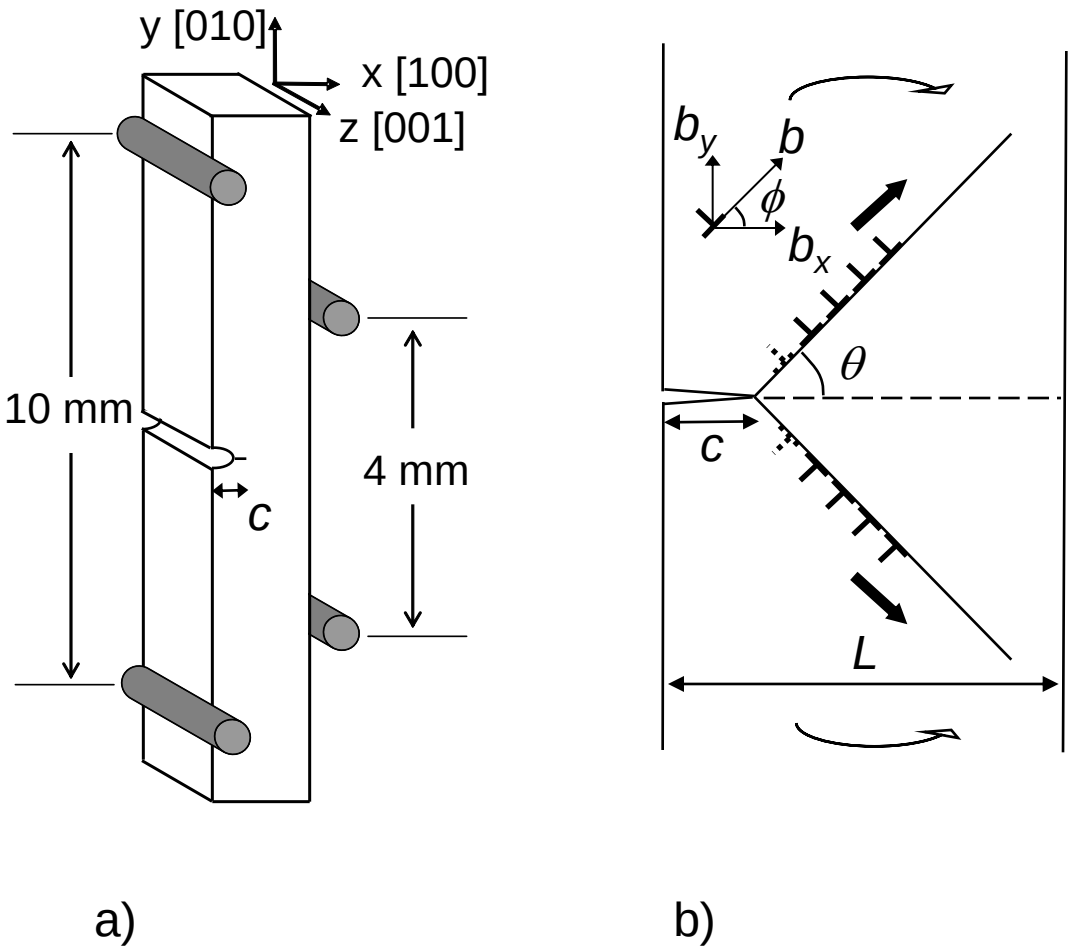

Figure 1: (a) Specimen geometry used in four-point bend fracture tests of single crystal iron. (b) The 2D model consists of a pair of slip planes at an angle θ =45° to the crack plane. Dislocations are nucleated at the two sources (dotted) placed 30 b from the crack-tip and move away from the tip allowing two dislocation arrays to form.

a)

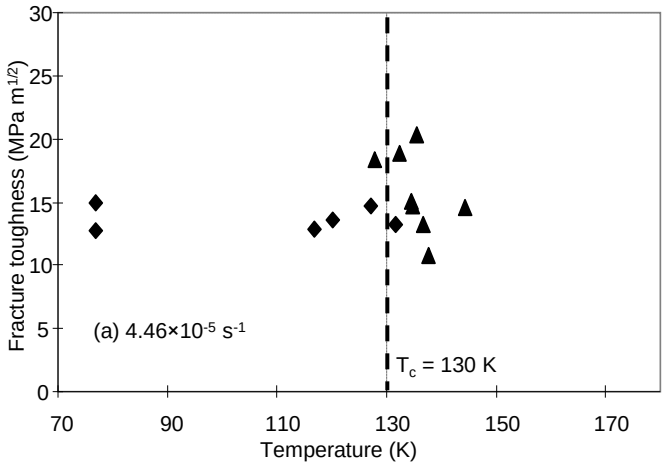

b)

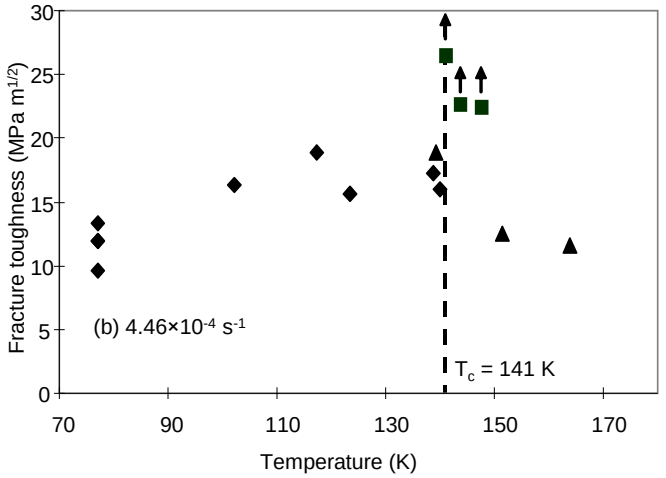

c)

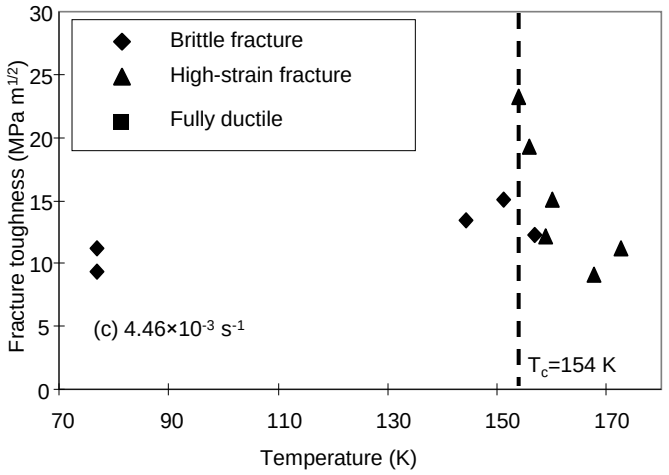

Figure 2
Experimental fracture toughness of single crystal iron as a function of test temperature at strain rates of:
(a) 4.46×10^{-3} s^{-1},
(b) 4.46×10^{-4} s^{-1}
(c) 4.46×10^{-5} s^{-1}.

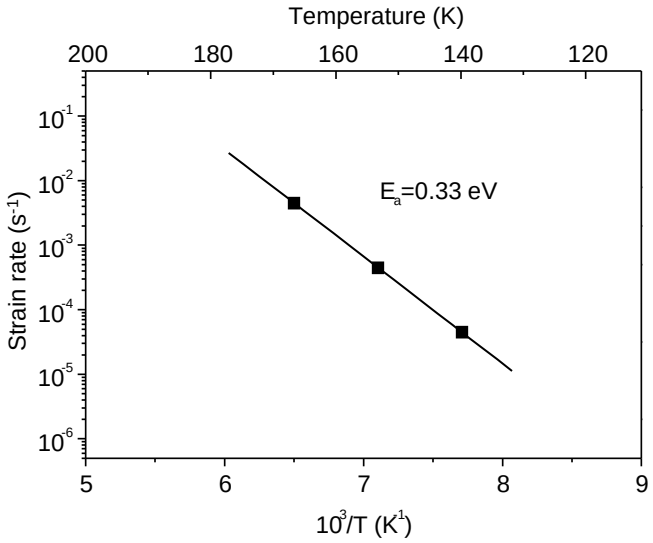

Figure 3: Arrhenius plot of reciprocal transition temperature in single crystal iron as a function of ln(strain rate).

a)

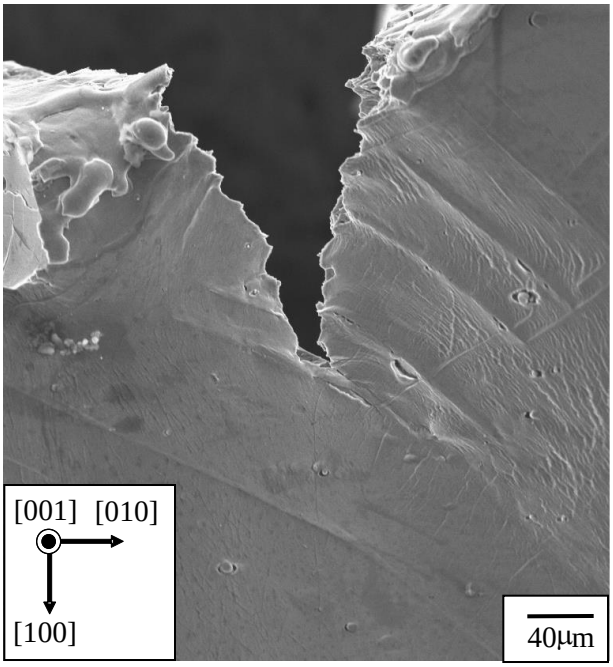

b)

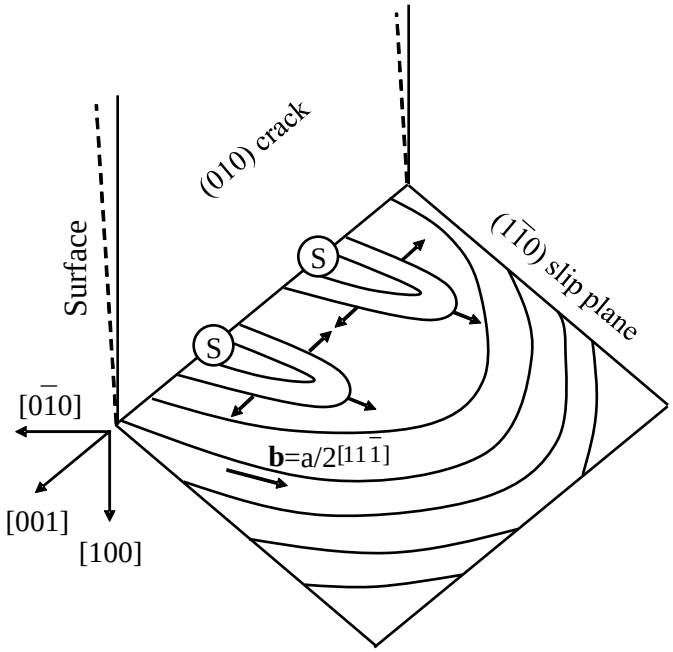

Figure 4
(a) Side view of a specimen tested at 144K and 4.46×10^{-4} s^{-1} (slightly above Tc); two types of slip bands are visible: straight lines aligned along <110> directions and wavy lines indicating cross slip.
(b) probable crack-tip dislocation configurations.

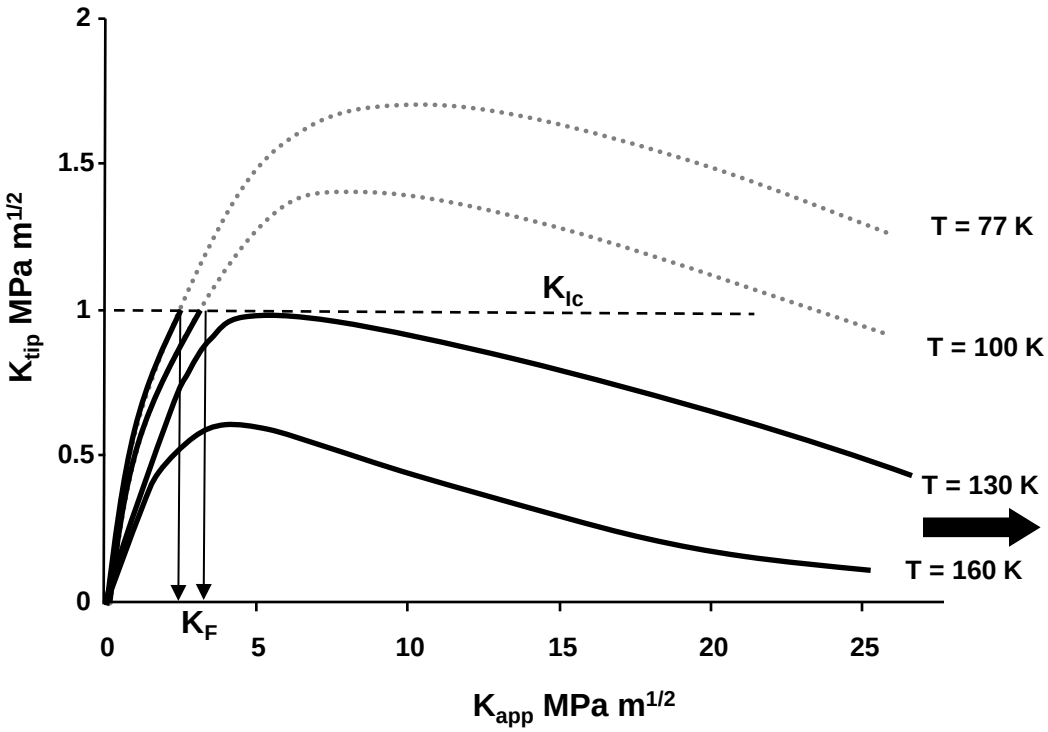

Figure 5: Predicted crack tip stress intensity K_{tip} as a function of applied stress intensity K_{app} at different temperatures at a loading rate of 4.46×10^{-5} s^{-1} Above a critical temperature (130 K in the figure), the fracture condition $K_{tip} = K_{Ic}$ is never met and the material is predicted to be ductile. Below this critical temperature, fracture is predicted to occur at an applied stress intensity $K_{app} = K_F$, higher than K_{Ic} due to the effects of dislocation shielding.

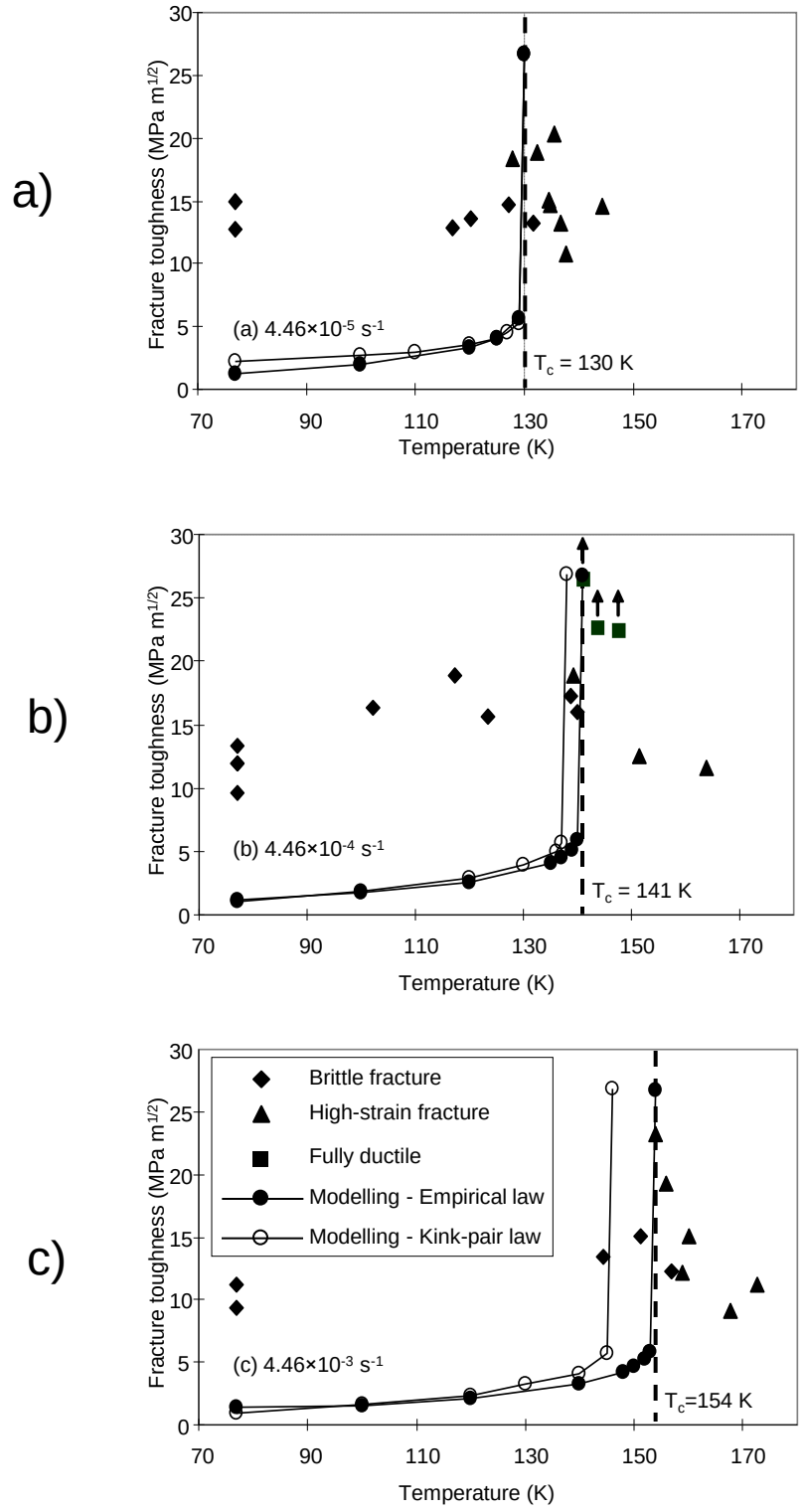

Figure 6
Experimental and modelled fracture toughness of single crystal iron as a function of test temperature at strain rates of:
(a) 4.46×10^{-3} s^{-1},
(b) 4.46×10^{-4} s^{-1}
(c) 4.46×10^{-5} s^{-1}.